Society of Medical Education & Research

2026, Volume 6, Issue 1, Page No: 301-321
ISSN: 3108-4834

Archive of International Journal of Cancer and Allied Science

# Engineering a Nanobody-Derived Trispecific T Cell Engager to Enhance T Cell Function and Reverse Immunosuppression in Solid Tumors

**Fatima El Idrissi[1]*, Samira Bennani[1], Youssef Benali[2], Ahmed Ben Ali[3]**

[1] Department of Trispecific T Cell Engagers and Solid Tumors, Faculty of Medicine, University of Marrakech, Marrakech, Morocco.
[2] Department of Nanobody Engineering and Immunotherapy, Faculty of Medicine, University of Fez, Fez, Morocco.
[3] Department of T Cell Function and Immunosuppression Reversal, Faculty of Medicine, University of Casablanca, Casablanca, Morocco.

***E-mail** ✉ fatima.idrissi@uca.ma

## Abstract

T cell engagers (TCEs) have emerged as an important therapeutic approach for hematologic malignancies, yet their effectiveness against solid tumors has been limited. Elevated expression of programmed cell death 1 (PD-1) is closely linked to T cell exhaustion and contributes to immunosuppression driven by the tumor. The creation of a novel nanobody-based trispecific T cell engager (Nb-TriTE) may offer an effective means to enhance treatment outcomes. Leveraging the favorable properties of nanobodies (Nbs), we first identified a nanobody specific for fibroblast activation protein (FAP). We constructed a Nb-based bispecific T cell engager (Nb-BiTE) directed at FAP. We then engineered a Nb-TriTE by linking an anti-PD-1 Nb to this Nb-BiTE. The functional properties and therapeutic potential of the Nb-TriTE were examined using in vitro assays and in vivo studies with both cell line- and patient-derived xenograft models in mice. We successfully isolated a FAP-specific Nb and used it to develop new Nb-BiTE and Nb-TriTE constructs that exhibited strong and specific binding to their intended targets. In vitro, the Nb-TriTE triggered efficient antigen-specific tumor cell killing, strong T cell activation, and improved T cell effector functions. In mouse models of multiple solid tumors, the Nb-TriTE also markedly reduced tumor progression, extended survival, and increased T cell infiltration into tumors compared with the Nb-BiTE, while demonstrating a favorable safety profile without detectable toxicity. The newly developed Nb-TriTE represents a versatile and promising platform capable of counteracting tumor-induced immunosuppression and potentially leading to better clinical results for patients in the future.

**Keywords:** Nanobody (Nb), Trispecific T cell engager (TriTE), Fibroblast activation protein (FAP), Programmed cell death 1 (PD-1), Solid tumor immunotherapy

## Introduction

Immunotherapy based on T cells is fundamentally changing oncology, and T cell engager (TCE) technology is a particularly promising strategy [1]. Bispecific T cell engagers (BiTEs) are among the most advanced and widely investigated formats within this class [2, 3]. Blinatumomab, the first approved BiTE targeting CD3 and CD19, has been approved by the FDA for the treatment of B-cell malignancies [4] and has demonstrated substantial efficacy in patients with blood cancers [5]. However, translating these benefits to solid tumors has proven difficult because of their heterogeneous nature and intricate biology [6, 7].

Many TCEs constructed with single-chain variable fragments (scFvs) exhibit poor folding efficiency and a propensity to aggregate, thereby reducing overall performance [8, 9]. Conventional TCE production is further complicated by challenges in properly assembling the heavy and light chain domains [9, 10]. Nanobodies (Nbs or VHHs), the smallest naturally occurring antigen-

Access this article online https://smerpub.com/

**Received:** 09 April 2026; **Accepted:** 28 June 2026



**How to cite this article:** El Idrissi F Bennani S, Benali Y, Ben Ali A. Engineering a Nanobody-Derived Trispecific T Cell Engager to Enhance T Cell Function and Reverse Immunosuppression in Solid Tumors. Arch Int J Cancer Allied Sci. 2026;6(1):301-21. https://doi.org/10.51847/D16JbH6T4N

binding units, have gained attention as superior building blocks for next-generation biologics [11]. The FDA approved the first nanobody therapeutic, caplacizumab, in 2019 [12]. Owing to their small size (~15 kDa), Nbs penetrate tissues rapidly and deeply [13, 14]. They are also insensitive to heavy-light chain mispairing issues that affect scFvs, allowing straightforward assembly into multispecific formats [8, 15-17]. In addition, Nbs preserve excellent target affinity and functionality, making them well-suited for clinical use [8, 18].

Previously, our laboratory introduced a nanobody-based BiTE (Nb-BiTE) platform targeting CD105 (endoglin), which demonstrated potent lysis of antigen-positive cells both in vitro and in xenograft mouse models [19]. Despite these encouraging preclinical findings, BiTE therapies—whether based on scFvs or Nbs—have encountered limited success in solid tumor trials, primarily due to the hostile immunosuppressive tumor microenvironment (TME) and the presence of dense stromal barriers [6, 20-22]. Therefore, strategies to further improve Nb-BiTE performance are essential.

Solid tumor development is typically associated with profound changes in the TME and increased expression of immune inhibitory receptors [23, 24]. In particular, the PD-1/PD-L1 axis plays a central role in restraining CD8+ T cell antitumor activity during immune escape [25, 26]. Blocking these checkpoint pathways has been shown to restore T cell function and effector capacity partially [27-31]. Because activated T cells frequently upregulate multiple inhibitory receptors that blunt BiTE activity in solid tumors, combining checkpoint blockade with BiTEs can reinvigorate long-lasting antitumor immunity. For instance, PD-1/PD-L1 inhibition has been found to augment the efficacy of the CD33/CD3 BiTE AMG 330 by mitigating T cell exhaustion [32, 33]. Integrating checkpoint blockade directly into BiTE molecules thus offers a logical approach to strengthen immune activation while preventing tumor evasion.

In this work, we designed an innovative nanobody-based trispecific T cell engager (Nb-TriTE) that incorporates three distinct Nbs: one specific for CD3ε on T cells, one for a tumor-associated antigen expressed on cancer-associated fibroblasts (CAFs), and a third targeting a critical immune checkpoint component. We propose that this tri-specific construct serves as molecular bridges that strengthen T cell engagement with CAFs, restore productive immune signaling, and thereby overcome local immunosuppression to promote effective tumor elimination. Target selection is critical for TCE success in solid tumors. CAFs highly express fibroblast activation protein (FAP) within the immunosuppressive TME of many solid cancers [34-39], while the PD-1/PD-L1 pathway represents a dominant mechanism of T cell inhibition [40]. A recent phase II study combining a FAP-targeted IL-2 variant with anti-PD-L1 therapy demonstrated encouraging activity in advanced squamous cell carcinoma (NCT03875079).

To realize this concept, we screened phage display libraries to obtain FAP-specific Nbs and constructed a corresponding Nb-BiTE. We then fused a previously characterized PD-1 Nb [41] to generate the Nb-TriTE. Our data indicate that the Nb-TriTE effectively redirects T cells to FAP-expressing CAFs and simultaneously relieves PD-1-mediated suppression, thereby facilitating stable immune synapse formation and enhancing T cell cytotoxicity against tumor cells. This study provides the first demonstration of such a Nb-TriTE platform, which holds considerable promise for amplifying TCE-mediated antitumor responses. The approach may also empower T cells to eradicate cancer cells more effectively. Collectively, this Nb-TriTE technology offers a broadly applicable TCE strategy that could translate into improved therapeutic outcomes for patients with solid tumors.

## Materials and Methods

*Cell culture and experimental animals*

HepG2, U87, PANC1, and 293T cell lines were maintained in Dulbecco's modified Eagle medium (DMEM) containing 10% fetal bovine serum (FBS) along with penicillin and streptomycin. Peripheral blood mononuclear cells (PBMCs) were obtained from healthy volunteers through Ficoll-based density gradient separation. Recombinant human IL-2 (PeproTech, UK) was included in T cell cultures at a final concentration of 300 IU/mL. Both PBMCs and Jurkat cells were grown in RPMI 1640 medium supplemented with 10% FBS, penicillin, and streptomycin. Stably transfected 293T-PD-1 and HepG2-FAP cells were cultured in DMEM with 10% FBS, penicillin, and streptomycin, and maintained in the presence of puromycin (1 μg/mL) for selection. All cultures were kept at 37 °C in a humidified incubator supplied with 5% $CO_2$.

Specific pathogen-free (SPF) nonobese diabetic/severe combined immunodeficiency (NOD/SCID) mice aged 4–6 weeks, lacking mature B and T lymphocytes, were obtained from Vital River Laboratory (Beijing, China)

and maintained under SPF conditions in our institutional animal facility. All in vivo experiments received prior approval from the Institutional Animal Care and Use Committee (IACUC) of Guangxi Medical University.

*Generation of nanobodies*

Nanobodies directed against FAP were isolated from phage display libraries using established screening procedures [19, 41-43]. His-tagged FAP Nbs were produced by induction with isopropyl β-D-1-thiogalactopyranoside (IPTG) (Solarbio, China) under optimized conditions and subsequently purified through $Ni^{2+}$–NTA affinity chromatography. Purity and integrity of the isolated Nbs were examined by sodium dodecyl sulfate–polyacrylamide gel electrophoresis (SDS–PAGE). Binding kinetics and affinity toward FAP were measured via surface plasmon resonance (SPR). In contrast, target recognition on cell surfaces was confirmed by flow cytometry using a FACS Canto flow cytometer (BD Biosciences, USA).

*Expression, purification and validation of Nb-TriTE*

Using standard molecular cloning techniques, the previously selected anti-hCD3ε Nb and anti-hPD-1 Nb [19, 41] were genetically connected to the anti-FAP Nb through a flexible $(GGGGS)_3$ linker. The complete construct was synthesized by GenScript Biotechnology Co., Ltd (Nanjing, China), subcloned into the pET-30a expression vector carrying His- and Flag-tags, and introduced into *E. coli* BL21 (DE3) cells. Bacterial cultures were expanded in 1 L Terrific Broth (TB) containing 50 μg/mL kanamycin at 37 °C until the optical density at 600 nm reached 2.0. Expression of Nb-TriTE was then induced by adding 0.5 mM IPTG, followed by incubation at 16 °C for 16 h. Cells were harvested by centrifugation at 12,000 rpm for 30 min, resuspended in phosphate-buffered saline (PBS), and disrupted by sonication. The resulting material was stored at −80 °C. Inclusion bodies were collected after extensive washing with PBS, solubilized in 8 M urea, refolded by gradual dialysis, and passed through a 0.22-μm sterile filter. The recombinant protein was further purified using a $Ni^{2+}$–NTA affinity resin (GenScript, China) according to the supplier's guidelines. Final protein quality was assessed by size-exclusion chromatography (SEC) and SDS–PAGE under reducing conditions, with visualization by Coomassie blue staining.

*Western blotting*

Nb-TriTE protein expression was verified by Western blot analysis employing an HRP-conjugated anti-His-tag antibody (Abcam, USA). Purified samples were separated by SDS–PAGE under reducing conditions and transferred to polyvinylidene fluoride (PVDF) membranes using a wet transfer system (Bio-Rad, USA). Membranes were blocked with 5% non-fat milk, incubated with the HRP-conjugated anti-His-tag antibody at a 1:3000 dilution, and developed with enhanced chemiluminescence substrate (BeyoECL Plus Lit, Beyotime, China). Chemiluminescent signals were captured and processed using Image Lab software (Bio-Rad, USA).

*Enzyme-linked immunosorbent assay (ELISA)*

Concentrations of IL-2, IFN-γ, TNF-α, granzyme B (GzmB), and perforin (PRF1) were quantified in serum and culture supernatants using commercially available ELISA kits (Liankebio, China for IL-2, IFN-γ, and TNF-α; Elabscience, China for GzmB and PRF1) according to the manufacturers' recommended protocols. In short, 100 μL aliquots of samples were added to wells and incubated with diluted detection antibodies for 2 h at 37 °C. Following washes with PBS containing 0.05% Tween 20 (PBST), HRP-conjugated avidin was applied for 45 min. Color development was initiated by adding the tetramethylbenzidine (TMB) substrate for 10 min, after which absorbance was measured at 450 nm on a microplate reader (Tecan, Mannedorf, Switzerland). Analyte concentrations were interpolated from standard curves generated in parallel.

PD-1/PD-L1 blockade activity of Nb-TriTE was determined by ELISA, with recombinant hPD-1 (ACRO, PD1-H5257) serving as the immobilized capture protein and biotinylated hPD-L1 (ACRO, PD1-H82E5) as the detection reagent. In addition, the ability of Nb-TriTE to bind multiple antigens simultaneously was evaluated using a sandwich ELISA format. Recombinant hFAP, hCD3ε, and hPD-1 proteins (ACRO, FAP-H5263, CDE-H5256, PD1-H5257) were used as capture agents, while the corresponding biotinylated versions (ACRO, FAP-H82Q6, CDE-H82E1, PD1-H82E4) served as detectors. Absorbance readings at 450 nm were obtained with a Tecan microplate reader (Mannedorf, Switzerland).

*Flow cytometry*

Target cell surface expression of FAP was evaluated following staining with a PE-labeled anti-human FAP antibody (R&D Systems, USA). Expression of PD-L1 on

target cells was similarly examined using an APC-conjugated anti-human PD-L1 antibody (Biolegend, USA). The binding capacity of Nb-TriTE at 2 μg/mL was tested in combination with a PE-conjugated anti-His-tag antibody (R&D Systems, USA). All samples were analyzed on a FACS Calibur flow cytometer (BD Biosciences, USA), and acquired data were interpreted with FlowJo software.

*T cell activation assay*

T cell activation in vitro was assessed by measuring surface marker expression and proliferative responses. Enriched T cells were co-incubated with target cancer cell lines at an effector-to-target ratio of 10:1 in the presence of Nb-TriTE or appropriate control agents. Following 24 h incubation at 37 °C, supernatants were harvested, and activation status was determined by quantifying the expression levels of CD25, CD69, and CD107a using PE-conjugated anti-CD69, PE-conjugated anti-CD25, and APC-conjugated anti-CD107a antibodies (Biolegend, USA). For memory phenotype analysis, parallel cultures were maintained for 14 days at 37 °C and then stained with PE-Cy7-conjugated anti-CD45RA and APC-conjugated anti-CD62L antibodies (Biolegend, USA) for 30 min at 4 °C. Flow cytometric acquisition was performed on a FACS Calibur instrument (BD Biosciences, USA), with subsequent data processing conducted using FlowJo software.

*Proliferation assay*

Assessment of T cell proliferative capacity was performed using the PKH26 dye-dilution method according to the supplier's guidelines (Sigma, USA). In summary, $1 \times 10^5$ tumor cells pretreated with mitomycin C were combined with PKH26-labeled PBMCs at an E:T ratio of 10:1 and cultured with Nb-TriTE or control compounds for 5 days. Proliferation was measured by flow cytometry and reported as the percentage decrease in PKH26 fluorescence intensity per cell generation.

*Cytotoxicity assay*

Redirected killing activity mediated by Nb-TriTE was quantified through a flow cytometry-based cytotoxicity assay. Target cells were pre-labeled with CFSE using a fluorescent cell tracking kit as instructed by the manufacturer (Invitrogen, USA). These labeled targets were then mixed with effector T cells at effector-to-target ratios of 1:1, 5:1, or 10:1 along with serial dilutions of Nb-TriTE or control molecules. Following 16 h of co-culture at 37 °C under 5% $CO_2$, cells were stained with propidium iodide (PI) (Sigma-Aldrich, USA) according to the manufacturer's protocol. The fraction of $CFSE^+PI^+$ cells was determined by flow cytometry and used to compute specific lysis according to the equation:

Specific lysis (%) = (fluorescence (sample lysis) − fluorescence (spontaneous lysis)) / (fluorescence (maximum lysis) − fluorescence (spontaneous lysis)) × 100.

*In vivo efficiency study*

Cell-derived xenograft (CDX) models were developed by subcutaneous injection of $1 \times 10^6$ HepG2-FAP cells per mouse or $1 \times 10^6$ PANC1 cells per mouse combined with CAFs (2:1 ratio) suspended in PBS into the lower back or axillary region of NOD/SCID mice. Seven days later, mice were randomly assigned to treatment groups (n = 5) and received an intravenous injection of $1 \times 10^7$ PBMCs in 100 μL PBS via the tail vein. Starting on the same day, animals were treated daily with 20 μg Nb-TriTE or with control agents intravenously for 6 consecutive days, while the vehicle control group received only PBS. Tumor dimensions were measured with calipers every 4 days, and volumes were calculated as (length × width$^2$)/2. Mouse body weights were monitored regularly. Animals were sacrificed when they showed substantial weight reduction, tumor ulceration, or when tumors reached a volume greater than 2000 mm$^3$.

For the orthotopic intracranial CDX model, anesthetized NOD/SCID mice were positioned in a stereotactic apparatus with a mouse-specific holder. Then, $1 \times 10^5$ U87 cells in 5 μL PBS were injected 2 mm lateral to the sagittal suture and 2 mm posterior to the bregma. Seven days after implantation, $1 \times 10^6$ PBMCs in 100 μL PBS were administered intravenously, followed by daily intravenous dosing of 20 μg Nb-TriTE or Nb-BiTE for six days. At termination, brains containing tumors were excised for histopathological assessment.

*Patient-derived tumor xenograft model*

Patient-derived xenograft (PDX) models were generated following methods outlined in prior reports [42, 44, 45]. In brief, freshly dissociated primary human liver cancer cells (P0) were mixed with Matrigel matrix (Corning, USA) and implanted subcutaneously into the flank or axilla of NOD/SCID mice (P1). Seven days post-engraftment, PBMCs were infused intravenously, and mice received daily intravenous injections of 20 μg Nb-TriTE or Nb-BiTE for six days. Tumor size was

measured with calipers every four days, and volumes were calculated using the same formula as above. In short-term experiments, tumors, spleens, and blood samples were collected for ex vivo evaluation. Selected tumor tissues were fixed in formalin, paraffin-embedded, and prepared for histological analysis and immunohistochemistry.

*RNA-seq assay*

RNA sequencing analysis was outsourced to Gene Denovo Biotechnology Co. Ltd. (Guangzhou, China). Total RNA was isolated from excised tumor tissues using TRIzol reagent (Invitrogen, USA) according to the manufacturer's protocol. RNA quality was evaluated by measuring the absorbance ratio at 260 nm to 280 nm (A260/A280), and integrity was further confirmed by electrophoresis on 1.5% agarose gels. Polyadenylated mRNA was enriched from the total RNA using oligo(dT) beads. Sequencing libraries were subsequently prepared from the enriched mRNA with the NEBNext Ultra RNA Library Prep Kit (New England Biolabs, #E7530, USA). Following end-repair of double-stranded cDNA fragments and ligation of Illumina adapters, the products were purified with AMPure XP Beads (1.0) and amplified by PCR. The completed libraries were sequenced on the NovaSeq 6000 platform (Illumina). Gene expression values were normalized and expressed as transcripts per million (TPM). Genes were classified as differentially expressed (DEGs) if they displayed a fold change exceeding two and an adjusted p-value below 0.05. Visualization of DEG patterns was achieved using heatmaps. Analysis of immune-related signatures relied on well-established public gene expression lists.

*Histological studies*

Apoptotic cells in tissue sections were detected using the terminal deoxynucleotidyl transferase dUTP nick-end labeling (TUNEL) method with a one-step assay kit (Beyotime, China) according to the manufacturer's directions. Immunohistochemical (IHC) evaluation of the Ki-67 proliferation marker was performed on paraffin-embedded sections after microwave antigen retrieval. Nonspecific binding and endogenous peroxidase activity were blocked with 3% hydrogen peroxide and goat serum. Sections were incubated with a ready-to-use anti-Ki67 antibody (MX006, MXB, China), followed by application of species-appropriate secondary antibodies according to established protocols. Staining signals were developed with diaminobenzidine (DAB) and imaged under a Nikon upright microscope.

In vivo safety of Nb-TriTE was examined by administering intravenous doses of either PBS vehicle or the Nb-TriTE construct to mice. Major organs (liver, heart, spleen, lung, and kidney) were harvested from euthanized animals, fixed in formalin, and processed into paraffin blocks. Thin 5-μm sections were prepared and stained with hematoxylin–eosin (HE) using routine histological techniques. Circulating levels of IL-6 and IL-1β in mouse serum were quantified using ELISA kits (Liankebio, China) according to the manufacturer's instructions. Serum biochemical parameters, including alanine aminotransferase (ALT) and aspartate transaminase (AST), were analyzed on an automatic biochemical analyzer (Catalyst One, IDEXX, USA).

*Statistical analysis*

Data analysis was performed using GraphPad Prism 9.0 (GraphPad, USA). For comparisons involving multiple experimental groups, one-way analysis of variance (ANOVA) was applied, followed by Tukey's multiple comparison test. Two-group differences were evaluated with Student's t test. Statistical significance was defined as $p < 0.05$, with levels indicated as * $P < 0.05$; ** $P < 0.01$; *** $P < 0.001$; **** $P < 0.0001$. All quantitative results are expressed as the mean ± standard deviation (SD).

## Results and Discussion

*Generation and verification of FAP Nbs*

Human FAP nanobodies (hFAP Nbs) were successfully isolated and purified using the established protocol described earlier [19, 41-43]. An overview of the production process is presented schematically **(Figure 1a)**. The initial PCR amplification produced the VHH-CH2 fragment at approximately 700 bp. This fragment then served as the template for a subsequent PCR reaction, yielding a VHH domain of approximately 400 bp. Following enzymatic digestion, the VHH sequences were ligated into pMECS vectors and introduced into *E. coli* TG1 cells by electroporation, resulting in an immune phage display library with a diversity of $2.25 \times 10^8$ CFU/mL, as quantified through colony counts on serially diluted plates. The accuracy of insert incorporation was confirmed by PCR screening of 24 randomly chosen colonies. Three rounds of affinity selection led to clear enrichment of clones specific for FAP compared with

background controls. From a panel of 96 colonies evaluated by phage ELISA, 24 demonstrated strong positivity (signal ratio exceeding 3). Six Nbs possessing distinct amino acid sequences were chosen for further characterization. SDS–PAGE analysis of the purified proteins revealed a predominant band near 15 kDa **(Figure 1b)**. Flow cytometry experiments confirmed specific recognition of FAP-positive cell lines (HepG2-FAP and U87), with no detectable interaction observed on FAP-negative HepG2 cells **(Figure 1c)**. Surface plasmon resonance (SPR) studies indicated excellent binding affinities, yielding dissociation constants (KD) in the range of $10^{-8}$ to $10^{-9}$ M **(Figure 1d)**. These data collectively confirm the successful establishment of a functional FAP-targeted Nb library. FAP Nb4 was selected for downstream experiments owing to its robust expression levels and favorable binding characteristics.

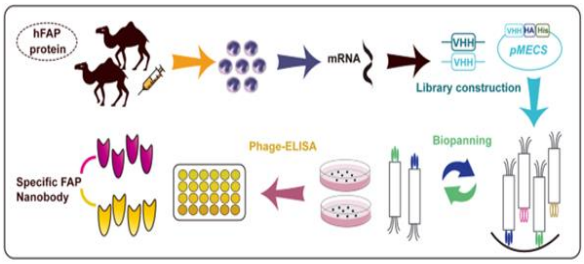


a)

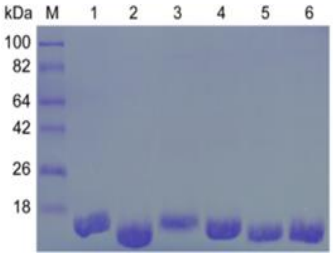


b)

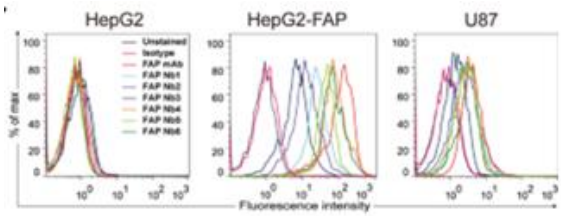


c)

| Name | $K_D$ (M) | | | | | |
|---|---|---|---|---|---|---|
| | FAP Nb1 | FAP Nb2 | FAP Nb3 | FAP Nb4 | FAP Nb5 | FAP Nb6 |
| hFAP | $4.10\times10^{-8}$ | $5.60\times10^{-8}$ | $1.08\times10^{-8}$ | $4.09\times10^{-8}$ | $1.53\times10^{-8}$ | $6.82\times10^{-9}$ |

d)

**Figure 1.** Construction of the Nb library and screening for hFAP-specific Nbs

(a) Overview of the procedural steps involved in generating hFAP-specific nanobodies, (b) Analysis of six purified hFAP Nbs by SDS–PAGE, (c) Flow cytometric evaluation demonstrating selective binding of hFAP Nbs to FAP-expressing HepG2-FAP and U87 cells, but not to FAP-negative HepG2 cells, and (d) Affinity measurements (KD values in molar units) of hFAP Nbs obtained through SPR.

*Design, generation and identification of the Nb-TriTE and Nb-BiTE*

A trispecific nanobody construct (Nb-TriTE) was engineered to direct T cells specifically toward FAP-positive cells while delivering localized blockade of the PD-1/PD-L1 inhibitory pathway. This was achieved by connecting an anti-PD-1 nanobody to a FAP-directed Nb-BiTE through a flexible (Gly4Ser)3 linker. A control molecule consisting of an irrelevant nontargeting Nb-BiTE/TriTE (Irrelevant ctr) was employed for comparative purposes. Three-dimensional structural models of both the Nb-TriTE and Nb-BiTE were predicted using homology modeling via the SWISS-MODEL platform (https://swissmodel.ExPASy.org) **(Figures 2a and 2d)**. The overall architecture of these nanobody-based molecules is distinct from that of conventional trispecific antibodies (TriAbs) [46] and other recently described TriTE formats [47], as is the case for the Nb-BiTE design.

Expression of the Nb-TriTE was carried out in *E. coli* BL21 (DE3) cells, with optimal yields obtained using 0.5 mM IPTG induction at 16 °C for 16 hours. The protein was extracted from bacterial inclusion bodies and refined through $Ni^{2+}$–NTA affinity purification. Both the Nb-BiTE and Nb-TriTE preparations displayed high purity (> 90%), as evidenced by a single major band on Coomassie-stained SDS–PAGE gels and size-exclusion chromatography profiles **(Figures 2b and 2e)**. Western blotting with an anti-His-tag antibody confirmed the expected molecular masses of approximately 35 kDa for Nb-BiTE and 50 kDa for Nb-TriTE **(Figures 2c and 2f)**. Different spatial arrangements of the PD-1 Nb and CD3ε Nb within the Nb-TriTE scaffold were tested to determine the optimal configuration. This was assessed by measuring cytokine secretion (IL-2 and IFN-γ) from stimulated T cells after 24 hours of incubation using ELISA. The configuration placing the PD-1 Nb in the proximal position and the CD3ε Nb in the distal position elicited the strongest T cell response. It was therefore

selected for assembly with the FAP Nb in the final Nb-TriTE molecule.

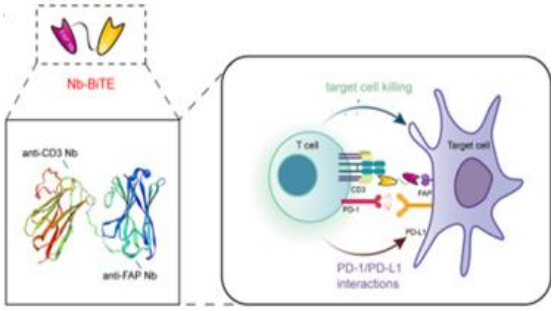


a)

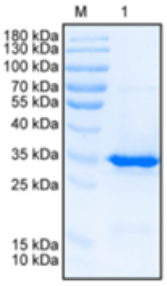


b)

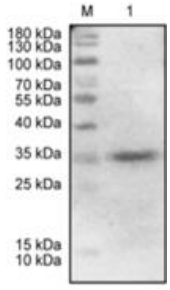


c)

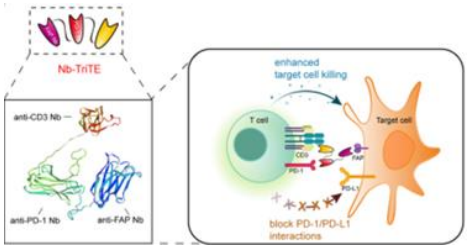


d)

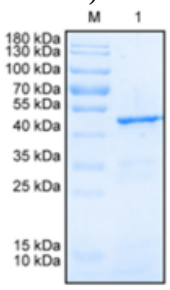


e)

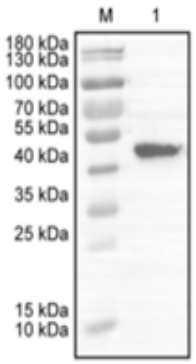


f)

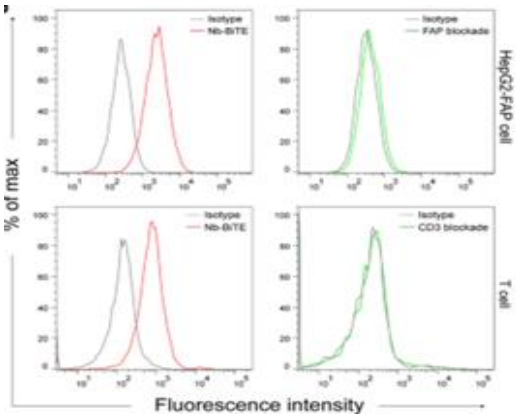


g)

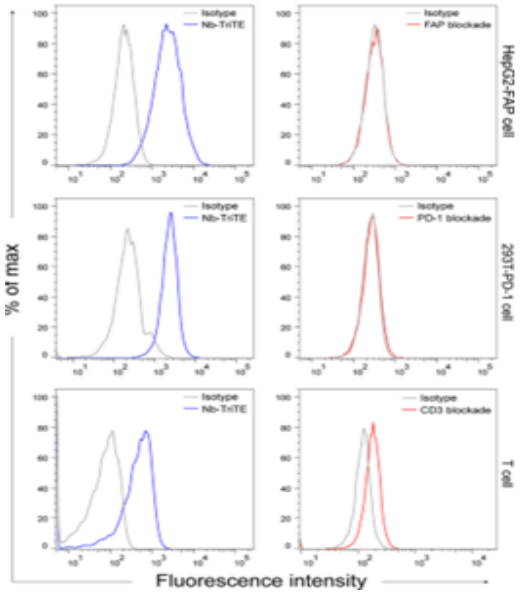


h)

| Name | KD (M) | | |
|---|---|---|---|
| | hFAP | hCD3 | hPD-1 |
| Nb-TriTE | 7.77E-08 | 1.04E-07 | 7.82E-07 |

i)

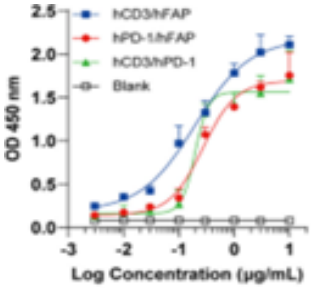


j)

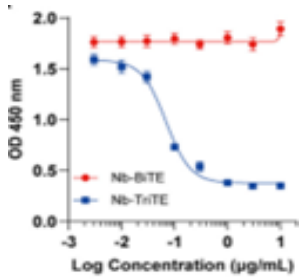


k)

**Figure 2.** Generation of Nb-TriTE and Nb-BiTE. Schematic illustrations of the Nb-BiTE (a) and Nb-TriTE (d) constructs, together with their predicted protein structures modeled using the SWISS-MODEL tool (www.ExPASy.org/resources/swiss-model). The Nb-BiTE comprises a FAP-specific Nb for recognition of cancer-associated fibroblasts and a CD3ε Nb for T cell engagement. The Nb-TriTE extends this design by addition of a PD-1 Nb to disrupt the PD-1/PD-L1 signaling axis, (b) Coomassie blue-stained SDS–PAGE of purified Nb-BiTE (M: molecular weight marker; lane 1: Nb-BiTE), (c) Western blot detection of purified Nb-BiTE with anti-His-tag antibody (M: molecular weight marker; lane 1: Nb-BiTE), (e) Coomassie blue-stained SDS–PAGE of purified Nb-TriTE (M: molecular weight marker; lane 1: Nb-TriTE), (f) Western blot detection of purified Nb-TriTE with anti-His-tag antibody (M: molecular weight marker; lane 1: Nb-TriTE), (g) Flow cytometry assessment of Nb-BiTE binding (2 μg/mL) to FAP-positive HepG2-FAP cells and CD3-positive human T cells, (h) Flow cytometry assessment of Nb-TriTE binding (2 μg/mL) to FAP-positive HepG2-FAP cells, PD-1-positive 293T-PD-1 cells, and CD3-positive human T cells. Representative histograms from antigen competition blocking experiments are also shown, and (i) SPR analysis of Nb-TriTE binding affinity, (j) Two-step sandwich ELISA demonstrating simultaneous binding of Nb-TriTE to antigen pairs (hCD3ε/hFAP, hPD-1/hFAP, and hCD3ε/hPD-1), and (K) ELISA-based evaluation of Nb-TriTE's ability to block the PD-1/PD-L1 interaction. Results are shown as mean ± standard deviation of three independent experiments.

*Binding properties of the Nb-TriTE and Nb-BiTE*

The interaction profiles of Nb-TriTE and Nb-BiTE with target cells were thoroughly investigated using flow cytometry and surface plasmon resonance (SPR). Data indicated that Nb-BiTE selectively recognized HepG2-FAP cells and primary human T cells, exhibiting no appreciable binding to unmodified HepG2 cells **(Figure 2g)**. In parallel, Nb-TriTE displayed targeted attachment to HepG2-FAP and 293T-PD-1 cells, while remaining non-reactive toward the parental HepG2 and 293T lines **(Figure 2h)**. The Nb-TriTE also showed clear recognition of CD3-positive primary T cells and Jurkat cells **(Figure 2h)**.

Specificity was further validated through competition experiments in which recombinant antigens were introduced to interfere with binding. Recombinant PD-1 protein effectively prevented Nb-TriTE attachment to 293T-PD-1 cells. Analogous inhibitory effects were noted when recombinant FAP or CD3ε proteins were applied in blocking assays for both constructs **(Figures 2g and 2h)**. Notably, inhibition by CD3ε alone proved less pronounced than that achieved by PD-1 blockade or dual PD-1/CD3ε blockade, indicating that Nb-TriTE could still access PD-1 molecules on T cells under select conditions.

Affinity measurements by SPR demonstrated that Nb-TriTE interacted with recombinant hFAP, hPD-1, and hCD3ε, with dissociation constants (KD) ranging from $10^{-7}$ to $10^{-8}$ M **(Figure 2i)**. Crucially, the molecule retained the ability to engage two distinct antigens concurrently, without substantial steric hindrance limiting accessibility **(Figure 2j)**. Additionally, Nb-TriTE inhibited the PD-1/PD-L1 association in a concentration-dependent manner, in contrast to the lack of activity observed with Nb-BiTE **(Figure 2k)**. Overall, these observations highlight the precise and multifunctional binding characteristics of the Nb-TriTE and Nb-BiTE molecules.

*Nb-TriTE-mediated T cell activation, proliferation and cytokine secretion*

Subsequent experiments evaluated the impact of Nb-TriTE and Nb-BiTE on T cell activation, expansion, and cytokine release. Engagement of T cells by these

molecules requires physical contact with target cells displaying the relevant antigens. Accordingly, expression of the early activation markers CD25 and CD69 was monitored to gauge stimulatory potential in vitro. As presented in **Figure 3**, T cells were co-incubated with HepG2-FAP cells in the presence of the test constructs. Treatment with Nb-TriTE led to substantially higher surface levels of CD25 and CD69 relative to Nb-BiTE or Nb-TriTE supplemented with soluble hPD-1 **(Figures 3a and 3b)**. The irrelevant control construct produced minimal activation. In addition, the degranulation marker CD107a was expressed at elevated levels exclusively in the Nb-TriTE group **(Figure 3c)**. These outcomes confirm that Nb-TriTE delivers strong activation signals, resulting in effective T cell responses.

Proliferation constitutes a key indicator of T cell responsiveness. Flow cytometric tracking of cell division after five days of co-culture revealed that Nb-TriTE triggered extensive proliferation of T cells when combined with mitomycin C-treated FAP-expressing tumor cells. This proliferative response was markedly greater than that observed with Nb-BiTE or Nb-TriTE plus hPD-1 **(Figure 3d)**. No division occurred in the presence of the irrelevant control or blank control conditions **(Figure 3e)**. Representative flow cytometry plots for activation markers and proliferation are displayed in **Figure 3e**.

Further characterization of the responding T cells involved assessment of CD62L and CD45RA to delineate memory subsets. Central memory T cells (TCMs; $CD45RA^{-}/CD62L^{+}$) are known for their superior proliferative capacity, lymphoid homing properties, and ability to generate effector cells upon antigen challenge. Exposure to Nb-TriTE increased the fraction of TCMs compared with Nb-BiTE treatment **(Figures 3f and 3g)**, suggesting the potential for more durable antitumor activity.

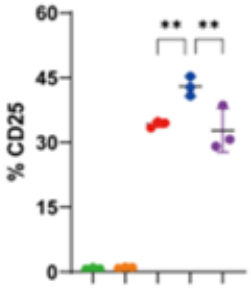


a)

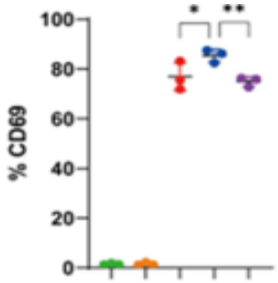


b)

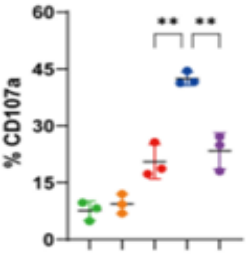


c)

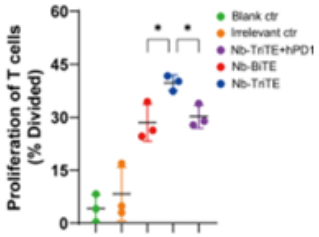


d)

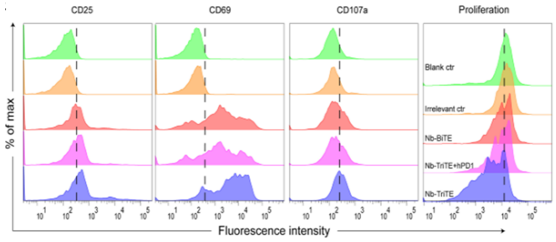


e)

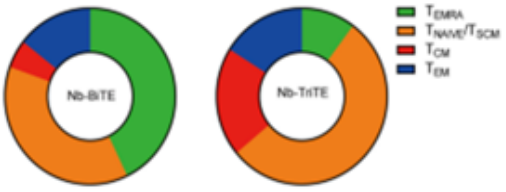


f)

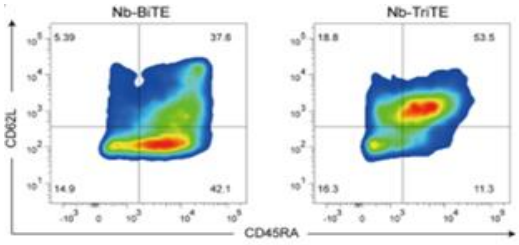


g)

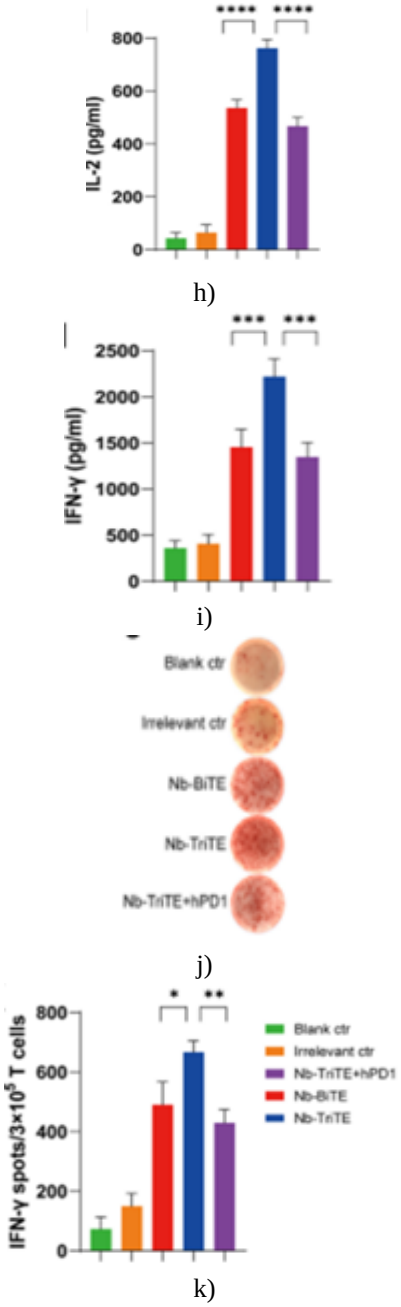


**Figure 3.** Nb-TriTE enhances T cell activation and function compared with Nb-BiTE. Induction of CD25 (a), CD69 (b), and CD107a (c) expression on T cells by Nb-TriTE versus controls, measured by flow cytometry after 24 h incubation with HepG2-FAP cells at an E:T ratio of 10:1 and 2 μg/mL protein concentration, (d) Assessment of T cell proliferation induced by Nb-TriTE relative to other treatments after 5 days of co-culture with HepG2-FAP cells at an E:T ratio of 10:1, reported as percentage of divided cells, (E) Representative flow cytometry histograms depicting CD25, CD69, and CD107a levels, and proliferation for the different groups. (F, G) Memory subpopulation profiling based on CD62L and CD45RA staining after 14 days of stimulation with Nb-TriTE or Nb-BiTE. $CD45RA^{-}CD62L^{-}$ cells indicate effector memory T (TEM) cells, $CD45RA^{-}CD62L^{+}$ cells indicate central memory T (TCM) cells, and $CD45RA^{+}CD62L^{+}$ cells indicate naive T cells. Pie charts illustrate the distribution of these subsets (left), (H, I) Quantification of secreted IL-2 and IFN-γ in supernatants from cultures containing HepG2-FAP cells treated with Nb-TriTE, Nb-BiTE, Irrelevant ctr, or Nb-TriTE + hPD-1 at matched molar concentrations, and (J-K) ELISPOT analysis of IFN-γ secretion by antigen-specific T cells across treatment groups. All results are expressed as mean ± standard deviation from three independent experiments.

Activated T cells also secrete proinflammatory cytokines that contribute to tumor elimination. Release of IL-2, IFN-γ, granzyme B (GzmB), and perforin (PRF1) was quantified following co-culture with target cells. Nb-TriTE induced significantly greater production of IL-2 and IFN-γ than Nb-BiTE, the combination of Nb-TriTE with hPD-1, or controls when FAP-positive cells were present **(Figures 3h and 3i)**. Cytokine output from Nb-BiTE was comparable to that of Nb-TriTE plus soluble hPD-1, while control treatments yielded lower levels. These differences were corroborated by ELISPOT assays detecting IFN-γ-secreting cells **(Figures 3j and 3k)**. When FAP-negative HepG2 cells were used, no meaningful elevation in IL-2 or IFN-γ secretion or IFN-γ spot formation was detected. Likewise, enhanced GzmB and PRF1 release by Nb-TriTE was observed only against FAP-positive targets, with no differences against FAP-negative cells.

In summary, Nb-TriTE proved superior in driving T cell activation and proliferation. This advantage is likely attributable to the integrated blockade of the PD-1/PD-L1 pathway within a single molecule, with target antigen specificity essential for its enhanced functional performance.

*Nb-TriTE-mediated cytotoxicity against FAP-positive tumor cells in vitro*

This study evaluated Nb-TriTE's capacity to trigger antigen-specific T cell cytotoxicity in vitro. It was proposed that the enhanced cytotoxic potency of Nb-TriTE would promote a stronger antitumor effect by facilitating PD-1/PD-L1 checkpoint blockade **(Figure**

**4a)**. Tumor cells and tissues were first analyzed for FAP and PD-L1 expression levels via flow cytometry, with public datasets confirming heterogeneous expression patterns across samples.

T cells were then co-cultured with target cells at an E:T ratio of 10:1 in the presence of increasing concentrations of purified Nb-TriTE, Nb-BiTE, or an irrelevant control. Nb-TriTE induced robust T cell-mediated killing of HepG2-FAP cells, achieving an EC50 of 0.63 nM, which was markedly lower than that of Nb-BiTE (EC50 of 7.5 nM) **(Figure 4c)**. No cytotoxicity was observed against FAP-negative HepG2 cells, confirming the strictly antigen-dependent and concentration-dependent nature of the response **(Figure 4b)**.

Nb-TriTE likewise demonstrated superior redirection of T cell cytotoxicity against other FAP-expressing targets compared with Nb-BiTE, including U87 cells (EC50 of 1.5 nM versus 5.19 nM) **(Figure 4d)** and primary CAFs (EC50 of 0.85 nM versus 17.48 nM) **(Figure 4e)**. Overall, Nb-TriTE produced significantly greater target cell lysis than Nb-BiTE, whereas the irrelevant control showed negligible activity.

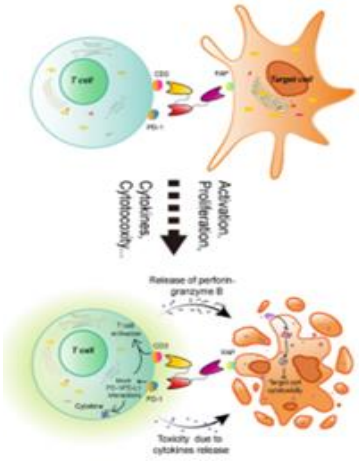


a)

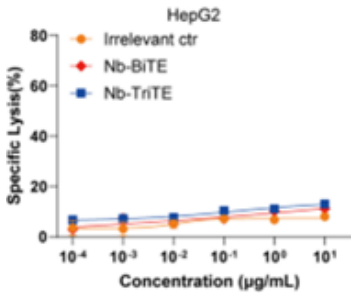


b)

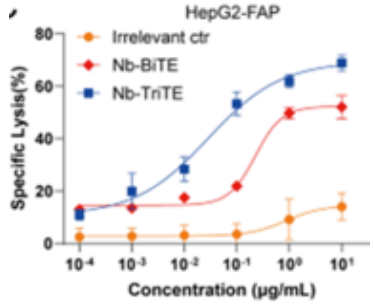


c)

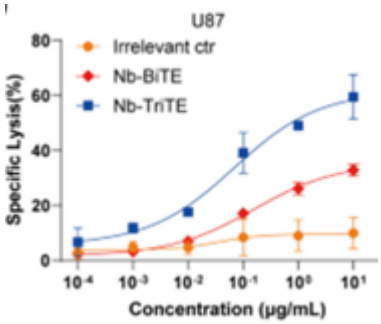


d)

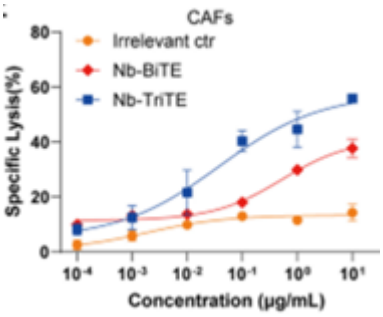


e)

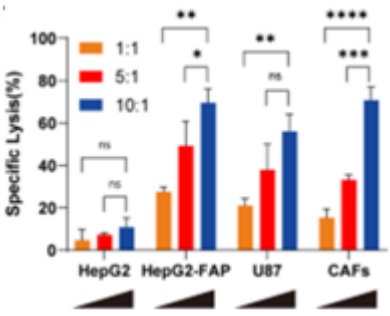


f)

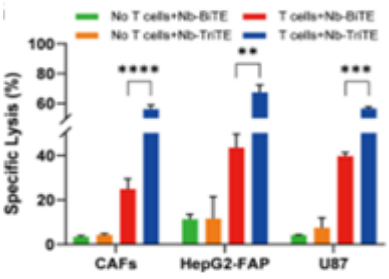


g)

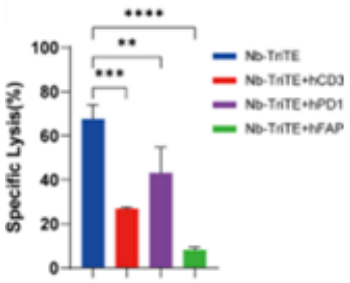


h)

**Figure 4.** Nb-TriTE promotes the antigen-specific lysis of FAP-expressing target cells by T cells in vitro

(a) Schematic illustration depicting the enhancement of tumor-specific cytotoxic T cell responses by Nb-TriTE through PD-1 blockade, (b–e) Concentration-dependent lysis of HepG2 versus HepG2-FAP cells, U87 cells, and primary CAF cells by unstimulated T cells, showing a direct relationship with Nb-TriTE concentration (E:T ratio 10:1; incubation time 16 h), (f) Nb-TriTE-induced cytotoxicity assays performed on target HepG2, HepG2-FAP, U87, and CAF cells at E:T ratios of 1:1, 5:1, and 10:1 over 16 h, (g) Cytotoxicity assays of target HepG2-FAP, U87, and CAF cells incubated with Nb-BiTE or Nb-TriTE, as well as Nb-BiTE (without T cells) or Nb-TriTE (without T cells), at an E:T ratio of 10:1 for 16 h, and (h) Cytotoxic lysis of HepG2-FAP cells mediated by Nb-TriTE and T cells at 2 μg/mL and an E:T ratio of 10:1 after 16 h, which is substantially diminished by individual blockade of hCD3ε, hPD-1, or hFAP.

Additional experiments confirmed that Nb-TriTE exhibited clear E:T ratio-dependent killing of FAP-positive cells, resulting in efficient lysis of FAP-expressing targets (HepG2-FAP, U87, and CAFs). No such enhancement occurred with FAP-negative HepG2 cells, underscoring the target cell specificity and E:T ratio dependence of Nb-TriTE activity **(Figure 4f)**. As expected, none of the constructs induced cytotoxicity in the absence of T cells. In the presence of T cells, however, Nb-TriTE displayed markedly superior killing compared with Nb-BiTE, verifying that the observed effect was T cell-dependent and driven by Nb-TriTE **(Figure 4g)**.

To distinguish between potential "cis"-crosslinking on the T cell surface and "trans"-bridging between T cells and target cells, control reagents were prepared (Nb-TriTE + hFAP, Nb-TriTE + hPD-1, and Nb-TriTE + hCD3). The data supported the notion that Nb-TriTE enhances T cell effector function primarily through a transcell-dependent mechanism **(Figure 4h)**. In summary, Nb-TriTE exerts potent cytotoxicity selectively against FAP-positive tumor cells, overcomes PD-1-associated resistance, and drives specific target cell lysis via synergistic PD-1/PD-L1 checkpoint inhibition.

*In vivo antitumor efficacy of Nb-TriTE in mouse xenograft models*

The in vivo therapeutic effectiveness of Nb-TriTE was subsequently investigated. CDX models were developed using FAP-expressing tumor types, including HepG2-FAP cells and a mixture of CAFs and PANC1 cells. On day 0, each mouse received a subcutaneous injection of $1 \times 10^6$ tumor cells in 100 μL PBS. Tumor-bearing animals were then randomly assigned to different treatment arms and given $1 \times 10^7$ T cells expanded from PBMCs through tail vein administration on day 7. Following T cell transfer, mice received daily intravenous injections of Nb-TriTE, Nb-BiTE, an irrelevant control, or PBS for 6 days **(Figures 5a and 5d)**.

Tumor growth curves in the PBS and irrelevant control cohorts progressed more rapidly than those in the Nb-TriTE and Nb-BiTE cohorts **(Figures 5b and 5e)**. Treatment with Nb-TriTE achieved the most pronounced tumor growth suppression and resulted in a notable increase in overall survival **(Figures 5c and 5f)**. An orthotopic glioma CDX model was additionally created by intracranial inoculation of U87 cells **(Figure 5g)**. In this setting, Nb-TriTE administration led to reduced tumor volumes within the brain and extended survival times compared with Nb-BiTE or PBS treatment **(Figures 5h and 5i)**, highlighting its preclinical therapeutic value. Across all three CDX models, no meaningful changes in body weight were observed among the treatment groups. These observations establish that Nb-TriTE successfully restrains tumor progression in vivo and enhances mouse survival. Further evaluation indicated superior tumor tissue infiltration by Nb-TriTE compared with standard TriAbs, accompanied by prolonged persistence. IHC analysis confirmed more extensive intratumoral distribution of Nb-TriTE compared with conventional TriAbs.

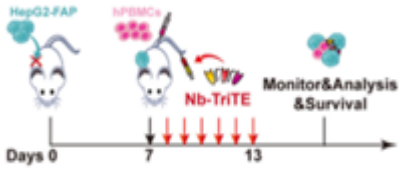


a)

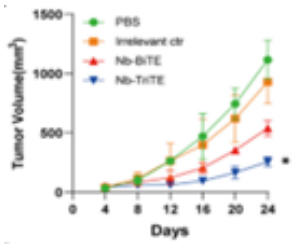


b)

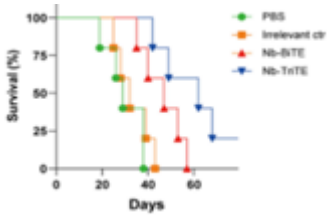


c)

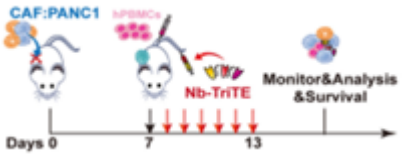


d)

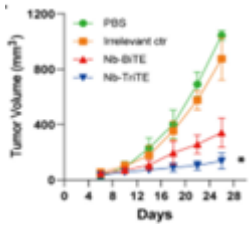


e)

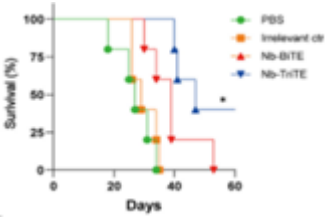


f)

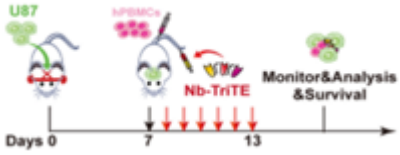


g)

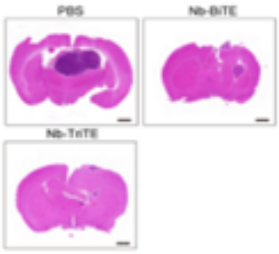


h)

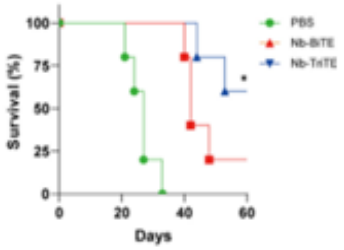


i)

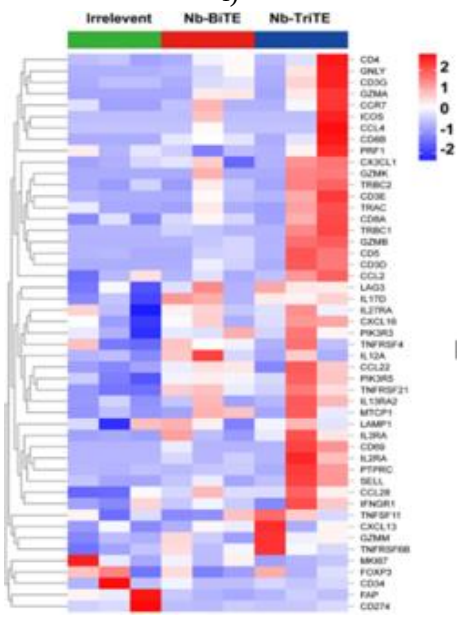


j)

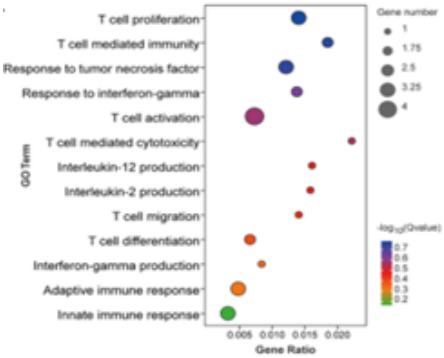


k)

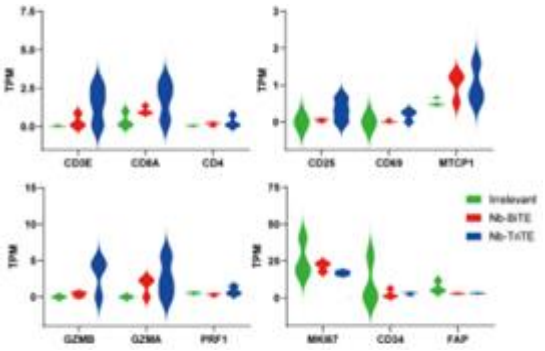


l)

**Figure 5.** Nb-TriTE administration augments antitumor activity in diverse cancer models

(a) Schematic summary of the study timeline. NOD/SCID mice (n = 5 per group) were subcutaneously injected with $1 \times 10^6$ HepG2-FAP tumor cells on day 0, infused intravenously with human PBMCs at a 1:10 ratio on day 7, and subsequently given Nb-TriTE or reference antibodies (20 μg) daily by intravenous route for a total of six doses, (b) Tumor volume growth curves, (c) Kaplan–Meier survival curves. (d) Schematic outline of the CAFs:PANC1 xenograft experimental setup, (e) Tumor volume curves. (f) Survival curves for CAFs:PANC1 tumors in NOD/SCID mice receiving the specified antibodies through daily intravenous delivery (n = 5 per group), (g) Schematic depiction of the orthotopic experimental procedure, (h) HE staining of brain tissue, (i) Survival curves of U87 tumors in NOD/SCID mice treated with the designated antibodies via daily intravenous infusion, (j) Heatmap illustrating expression profiles of selected genes in tumor tissues harvested from mice treated with irrelevant control, Nb-BiTE, or Nb-TriTE, (k) GO enrichment analysis performed on differentially expressed genes from tumor tissues of Nb-BiTE-treated versus Nb-TriTE-treated mice, and (l) Relative quantification of gene expression using TPM for markers linked to T cell activation, proliferation, and cytotoxicity (n = 3 independent biological replicates).

To better understand how Nb-TriTE enhances immune effector functions, RNA-seq was performed on CAFs:PANC1 tumor samples from the Nb-TriTE cohort to delineate the underlying transcriptional changes **(Figure 5j)**. DEGs characteristic of Nb-TriTE treatment were determined. Comparative GO enrichment analysis between Nb-BiTE and Nb-TriTE groups demonstrated that genes upregulated in the Nb-TriTE arm were strongly associated with T cell proliferation and activation, T cell-mediated immune responses and cytotoxicity, and the production of proinflammatory cytokines including TNF, IFN-γ, and IL-2 **(Figure 5k)**. Signature gene analysis further showed elevated expression of critical genes governing T cell activation, proliferation, and cytotoxic activity in Nb-TriTE-treated tumors relative to Nb-BiTE and control groups **(Figure 5l)**. Representative examples encompass T cell lineage markers (CD3E, CD8A, CD4), activation indicators (CD25, CD69), proliferation regulators (MTCP1), and effector molecules (GzmB, GzmA, PRF1). Conversely, proliferation- and angiogenesis-related tumor genes (MKI67, CD34) and CAF markers (FAP) showed reduced expression in the Nb-TriTE group.

In conclusion, Nb-TriTE effectively controls tumor growth in living animals and prolongs survival by stimulating T cell activation and amplifying their cytotoxic capabilities.

To better reflect the physiological milieu of tumor progression in living systems, researchers developed a PDX model using tissue from a patient with liver cancer **(Figure 6a)**. Flow cytometry of the PDX tumors revealed elevated FAP and PD-L1 expression. In this liver cancer PDX setting, daily repeated dosing with Nb-TriTE led to clear suppression of tumor growth and prolonged animal survival compared with groups treated with Nb-BiTE or PBS **(Figures 6b and 6c)**. Body weight profiles showed no substantial fluctuations before or after therapy in either experimental model. Tumor volume progression observed in the PDX model is presented in the corresponding line graph.

Assessment of Nb-TriTE interaction with T cells isolated from treated animals indicated moderate binding to T cells within the initial 24 h period **(Figure 6d)**. Monitoring of circulating cytokines further revealed temporary increases in the concentrations of IL-2, IFN-γ, and TNF-α among NOD/SCID mice that received Nb-TriTE **(Figures 6e–6g)**. Additional investigations into the capacity of Nb-TriTE to enhance immune cell recruitment showed that animals administered Nb-TriTE had greater numbers of human CD3+ CD8+ T cells in both tumor and spleen tissues than those given Nb-BiTE or PBS **(Figurers 6h, 6j and 6k)**. Peripheral blood analysis by flow cytometry similarly identified a notably higher proportion of CD3+ T cells in the Nb-TriTE cohort during the two weeks following administration.

Tumor specimens from all treatment arms underwent TUNEL and Ki67 immunohistochemical evaluation **(Figure 6i)**. The Nb-TriTE group displayed significantly

fewer Ki67-positive proliferating cells and a higher frequency of apoptotic cells as revealed by the TUNEL assay when compared with the Nb-BiTE and PBS cohorts **(Figures 6l and 6m)**. In summary, data from the PDX model support the potential of Nb-TriTE as an effective anticancer modality. Overall, these observations underscore the value of this innovative Nb-TriTE design as a robust therapeutic platform that delivers improved treatment outcomes.

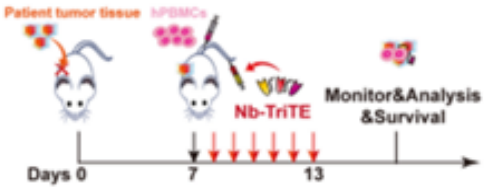


a)

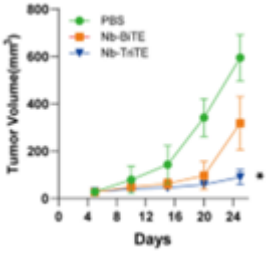


b)

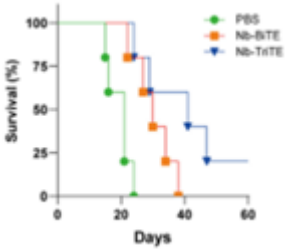


c)

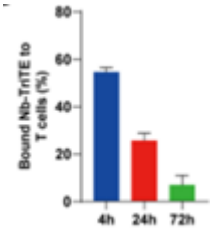


d)

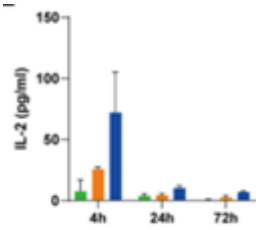


e)

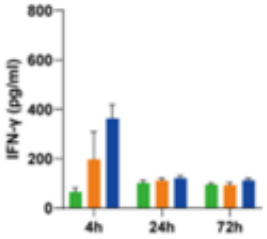


f)

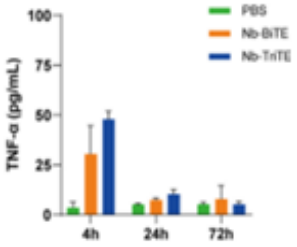


g)

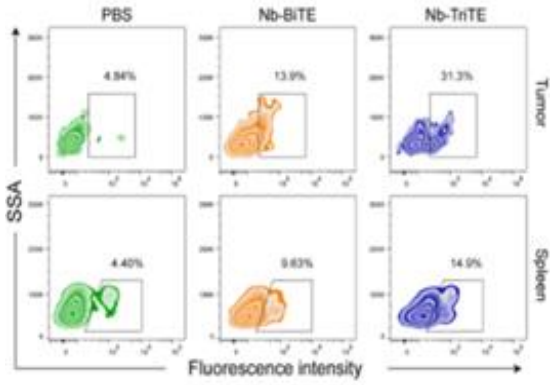


h)

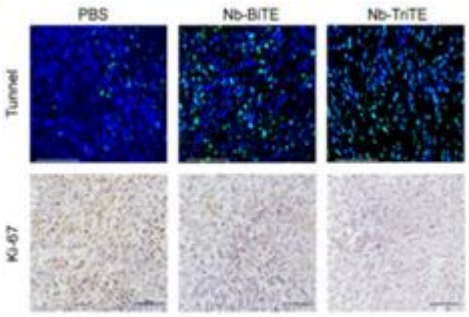


i)

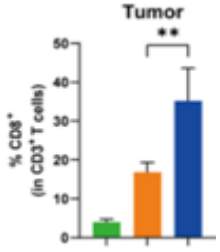


j)

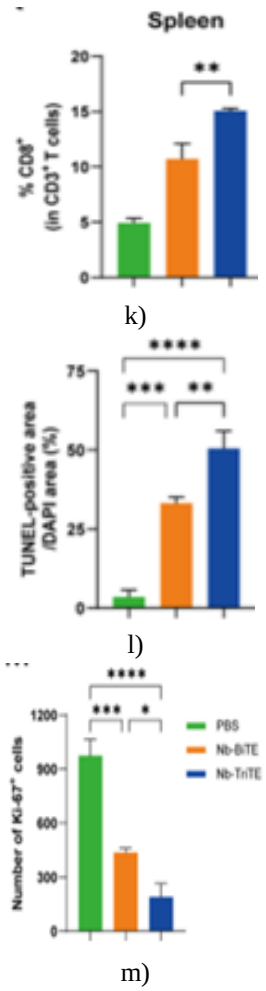


k)

l)

m)

**Figure 6.** Nb-TriTE administration robustly restrains the expansion of PDX tumors

(a) Schematic illustration of the PDX tumor model experimental protocol. Tumor growth curves (b) and survival curves (c) for PDX models (n = 5 per group) subjected to daily Nb-TriTE or Nb-BiTE treatment over six consecutive days. (d) Time-dependent alterations in the percentage of T cells associated with Nb-TriTE during the 72 h period after administration. (e–g) Circulating levels of IL-2 (e), IFN-γ (f), and TNF-α (g) in mice treated with Nb-TriTE or Nb-BiTE. Quantification of CD3+ CD8+ T cell infiltration in tumor and spleen tissues by flow cytometry, including representative density plots (h) and corresponding quantitative summaries (j, k). Assessment of tumor tissues by TUNEL and Ki67 staining. Representative photomicrographs (i) and quantitative analyses (l, m). Scale bars for TUNEL: 125 μm; scale bars for Ki67 IHC: 100 μm (n = 3 per group).

*Safety profile of Nb-TriTE*

The safety characteristics of Nb-TriTE were next evaluated. Although the treated mice showed no clinical signs of distress or adverse effects, comprehensive histopathological examination of major organs—including the heart, liver, spleen, lung, and kidney—was performed using HE staining. Results showed no evidence of pathological lesions or organ damage in animals receiving Nb-TriTE compared with those in the PBS control group **(Figure 7f)**.

Serum biochemical analysis further demonstrated that Nb-TriTE treatment did not cause statistically significant elevations in ALT or AST concentrations, or in the ALT/AST ratio **(Figures 7a–7c)**. Likewise, no notable differences in circulating levels of the proinflammatory cytokines IL-6 **(Figure 7d)** and IL-1β **(Figure 7e)** were observed between the Nb-TriTE and PBS groups. Taken together, these observations confirm that Nb-TriTE possesses a well-tolerated safety profile in mice. Overall, the findings establish the safety of this agent and provide strong justification for its continued development in clinical settings.

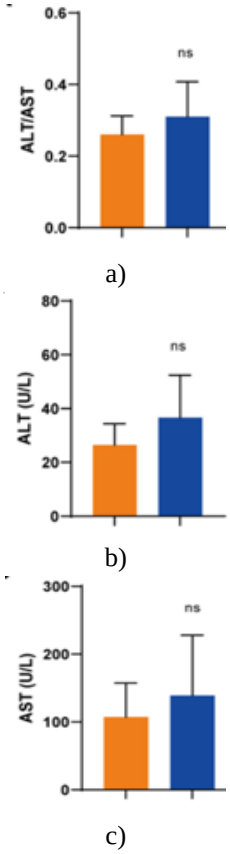


a)

b)

c)

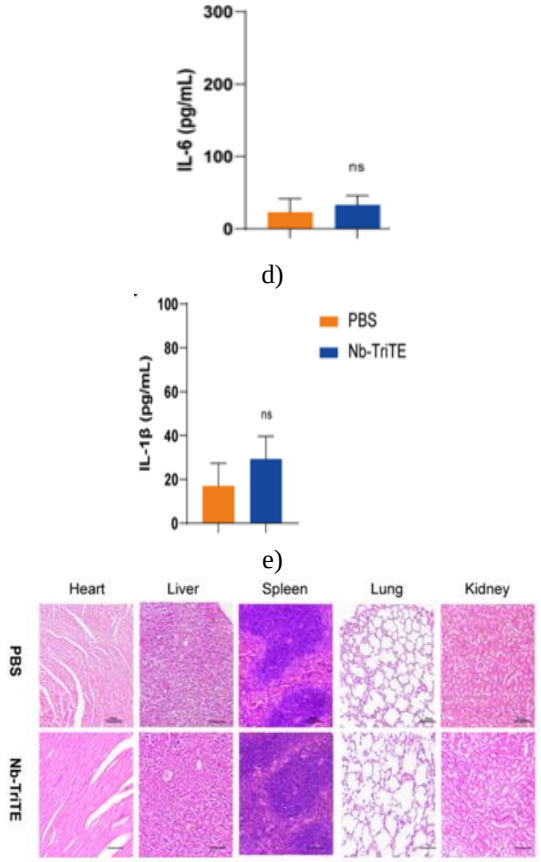


**Figure 7.** Preliminary safety evaluation of Nb-TriTE. ALT/AST ratios

(a), ALT levels (b), and AST levels (c) recorded during the study. Serum concentrations of IL-6 (d) and IL-1β (e) post-treatment, and (f) Representative micrographs of HE-stained sections from key organs (heart, liver, spleen, lung, kidney) across treatment conditions. Scale bar, 100 μm. No significant histopathological differences were detected following Nb-TriTE administration.

Advancing novel TCE designs is essential to overcome the substantial hurdles associated with conventional BiTE therapies in the treatment of solid tumors. The current investigation introduced Nb-TriTE, an innovative multispecific platform featuring three independent antigen-binding domains. This construct simultaneously engages T cells, tumor-associated antigens, and immune checkpoint molecules, offering the potential to reshape the immunosuppressive tumor microenvironment and restore productive antitumor T cell responses **(Figures 8a–8d)**. Nb-TriTE is the inaugural Nb-only trispecific candidate that simultaneously targets CD3ε, a solid tumor target, and an immune checkpoint receptor. Its molecular design sets it apart from previously described trispecific entities such as TriTE [47], TriTAC [48, 49], DARPin [34], CiTE [33], and other multispecific antibodies explored in cancer immunotherapy [46]. These developments mark a meaningful progression beyond existing immunotherapeutic strategies.

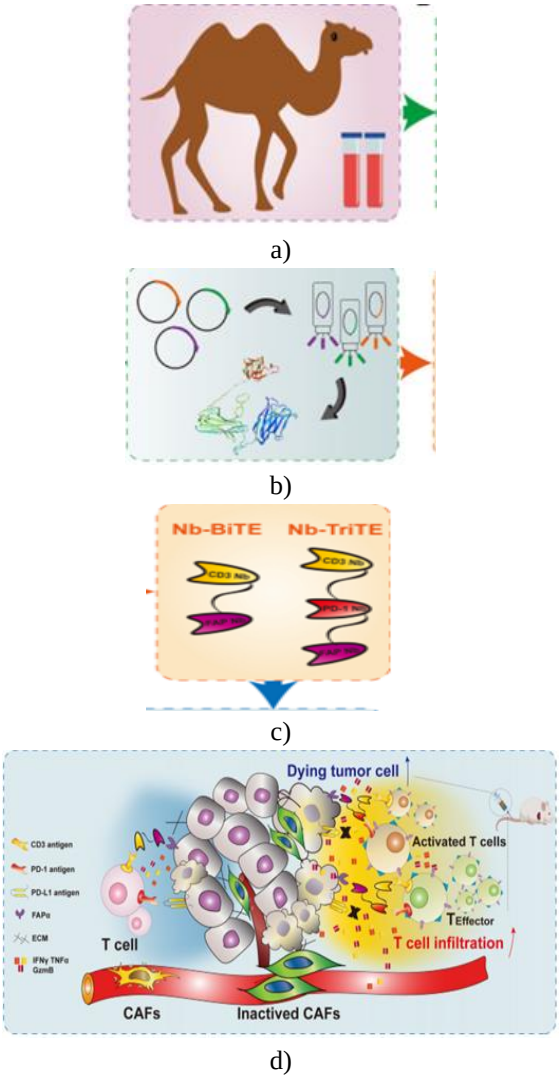


**Figure 8.** Schematic representation of the superior antitumor mechanism driven by Nb-TriTE

(a, b) Generation of Nb components, (c) Assembly and structural organization of Nb-BiTE and Nb-TriTE, and (d) Functional model illustrating the mode of action of Nb-BiTE versus Nb-TriTE.

Effective T cell immunity forms a cornerstone of solid tumor immunotherapy. Cancer cells commonly evade immune recognition by exploiting immunosuppressive pathways that compromise T cell functionality and

support tumor dissemination [50, 51]. Conventional TCE approaches have largely concentrated on tumor antigen engagement for direct cytotoxicity, often neglecting the need to counteract the broader immunosuppressive tumor microenvironment and restore exhausted T cell populations. Inhibitory signaling via immune checkpoint pathways potently dampens T cell activation, leading to progressive dysfunction of CD8+ T cells. Recent observations indicate that solid tumors can resist BiTE-mediated killing by upregulating PD-1/PD-L1 and delivering inhibitory signals to T cells [52-54]. Accordingly, assessment of PD-L1 status in tumor specimens may hold predictive value for clinical response to Nb-TriTE.

Publicly accessible datasets highlight strong correlations between FAP expression and immune features in various malignancies. Single-cell profiling further localizes FAP predominantly to CAFs in PAAD samples. The frequent overexpression of FAP on CAFs across many solid cancers suggests that targeted elimination of these stromal cells could confer therapeutic benefit. This premise underpins the dual-targeting design of Nb-TriTE, which redirects T cell cytotoxicity toward both malignant cells and suppressive CAFs. FAP-positive CAFs have also been implicated in conferring resistance to anti-PD-1/PD-L1 therapies [55], further supporting the integration of anti-FAP and anti-PD-1 VHH domains into a single molecule. Exploring Nb-based constructs to disrupt checkpoint-mediated inhibition therefore emerges as a valuable strategy to potentiate T cell activity and TCE performance.

Nanobodies possess highly attractive attributes for therapeutic development, including superior stability, high affinity, facile recombinant production, scalability, and economic viability. This study successfully isolated and characterized a FAP-specific Nb that displays strong target selectivity and binding potency. Six candidate FAP Nbs were rigorously tested by flow cytometry and surface plasmon resonance, and FAP Nb4 was selected for its balanced affinity and favorable expression characteristics. Previously generated PD-1- and CD3ε-specific Nbs [19, 41] complemented this panel. The identification of these high-quality Nb modules establishes a robust basis for future monospecific and multispecific Nb-derived therapeutics.

Leveraging these components, the Nb-TriTE platform was constructed to engage FAP on CAFs, CD3ε on T cells, and PD-1 on immune cells. Both Nb-TriTE and Nb-BiTE variants demonstrated appropriate specificity and binding strength. Functional evaluation showed that Nb-TriTE more potently stimulated T cell proliferation, activation, and cytotoxicity in vitro than its bispecific counterpart, and achieved greater tumor control across several solid tumor xenograft models in vivo. Experiments using soluble hPD-1 protein revealed reduced T cell activation, proliferation, and cytokine production when PD-1 engagement was competed, confirming the contribution of checkpoint blockade to Nb-TriTE activity. In vitro cytotoxicity assays established that Nb-TriTE triggers efficient, concentration-dependent, and strictly antigen-restricted killing of FAP-positive tumor cells, sparing FAP-negative targets. PD-1 blockade studies emphasized the essential role of checkpoint inhibition in sustaining durable T cell responses against solid tumors. Overall, these data illustrate that Nb-TriTE exhibits favorable binding properties and affinity, supporting the broad translational potential of Nb-derived TCEs as standalone agents or components of combination immunotherapies. The present findings indicate that Nb-BiTE treatment produces only modest antitumor activity in vivo compared with Nb-TriTE. In contrast, Nb-TriTE elicits robust therapeutic responses both in vitro and in vivo. These outcomes highlight the advantage of incorporating PD-1 blockade to reinvigorate T cell function, thereby generating stronger antitumor immunity and establishing a more efficient immunological bridge between T cells and CAFs. In patient-derived xenograft models, Nb-TriTE demonstrated superior tumor control compared with Nb-BiTE, accompanied by enhanced infiltration of CD3+CD8+ T cells into tumor tissue and the spleen. Immune checkpoint blockade not only reverses T cell exhaustion but also influences additional immune populations, including dendritic cells. Preliminary safety evaluations confirmed that Nb-TriTE exhibits a favorable toxicity profile.

Beyond the Nb-TriTE and Nb-BiTE platforms, combining Nb-based approaches with other modalities—such as CAR-T cell therapy, oncolytic viruses [56], vaccines [57], and additional immune checkpoint inhibitors—holds considerable promise for optimizing cancer immunotherapy outcomes.

Although encouraging tumor regression was achieved in subcutaneous and orthotopic NOD/SCID models, further translational studies are warranted to facilitate clinical advancement. Future optimization may include extending the circulating half-life of Nb-TriTE by fusing it to an albumin-binding Nb, thereby enabling less

frequent dosing and improved patient compliance. Although Nbs generally display low immunogenicity, standard humanization procedures should be applied to support clinical development. Additional preclinical evaluation in immunocompetent huCD3ε humanized mouse models could provide valuable insights into factors influencing therapeutic efficacy. Furthermore, single-cell RNA sequencing would provide greater resolution into the transcriptional programs activated following Nb-TriTE administration. At present, the detailed contribution of Nb-TriTE to specific T cell effector pathways remains incompletely characterized, necessitating continued mechanistic investigations in vivo.

## Conclusion

This study introduces a novel Nb-TriTE platform that integrates T cell engager technology with immune checkpoint blockade to effectively counteract tumor-induced immunosuppression. The results establish Nb-TriTE as a safe and potent therapeutic approach capable of generating targeted, antigen-specific T cell responses that restrain tumor progression. The modular and adaptable nature of this Nb-TriTE platform enables broad applicability and straightforward customization for diverse tumor types. Consequently, Nb-TriTE constitutes a valuable addition to the expanding repertoire of T cell engager-based immunotherapies, with significant implications for both fundamental immunology research and clinical oncology.

**Acknowledgments:** None

**Conflict of Interest:** None

**Financial Support:** None

**Ethics Statement:** None

## References

1. Goebeler ME, Bargou RC. T cell-engaging therapies—BiTEs and beyond. Nat Rev Clin Oncol. 2020;17(7):418-34.
2. Dagher OK, Schwab RD, Brookens SK, Posey AD Jr. Advances in cancer immunotherapies. Cell. 2023;186(8):1814-e1.
3. Wolf E, Hofmeister R, Kufer P, Schlereth B, Baeuerle PA. BiTEs: bispecific antibody constructs with unique anti-tumor activity. Drug Discov Today. 2005;10(18):1237-44.
4. Wu J, Fu J, Zhang M, Liu D. Blinatumomab: a bispecific T cell engager (BiTE) antibody against CD19/CD3 for refractory acute lymphoid leukemia. J Hematol Oncol. 2015;8(1):104.
5. Tian Z, Liu M, Zhang Y, Wang X. Bispecific T cell engagers: an emerging therapy for management of hematologic malignancies. J Hematol Oncol. 2021;14(1):75.
6. de Miguel M, Umana P, GomesdeMorais AL, Moreno V, Calvo E. T-cell-engaging therapy for solid tumors. Clin Cancer Res. 2021;27(6):1595-603.
7. Edeline J, Houot R, Marabelle A, Alcantara M. CAR-T cells and BiTEs in solid tumors: challenges and perspectives. J Hematol Oncol. 2021;14(1):65.
8. Bannas P, Hambach J, Koch-Nolte F. Nanobodies and nanobody-based human heavy chain antibodies as antitumor therapeutics. Front Immunol. 2017;8:1603.
9. Worn A, Pluckthun A. Stability engineering of antibody single-chain Fv fragments. J Mol Biol. 2001;305(5):989-1010.
10. Enderle L, Shalaby KH, Gorelik M, Weiss A, Blazer LL, Paduch M, et al. A T cell redirection platform for co-targeting dual antigens on solid tumors. MAbs. 2021;13(1):1933690.
11. Hamers-Casterman C, Atarhouch T, Muyldermans S, Robinson G, Hamers C, Songa EB, et al. Naturally occurring antibodies devoid of light chains. Nature. 1993;363(6428):446-8.
12. Jovcevska I, Muyldermans S. The therapeutic potential of nanobodies. BioDrugs. 2020;34(1):11-26.
13. Sun S, Ding Z, Yang X, Zhao X, Zhao M, Gao L, et al. Nanobody: a small antibody with big implications for tumor therapeutic strategy. Int J Nanomed. 2021;16:2337-56.
14. Verhaar ER, Woodham AW, Ploegh HL. Nanobodies in cancer. Semin Immunol. 2021;52:101425.
15. Asaadi Y, Jouneghani FF, Janani S, Rahbarizadeh F. A comprehensive comparison between camelid nanobodies and single chain variable fragments. Biomarker Res. 2021;9(1):87.
16. Maali A, Gholizadeh M, Feghhi-Najafabadi S, Noei A, Seyed-Motahari SS, Mansoori S, et al. Nanobodies in cell-mediated immunotherapy: on the

road to fight cancer. Front Immunol. 2023;14:1012841.
17. Wang J, Kang G, Yuan H, Cao X, Huang H, de Marco A, et al. Research progress and applications of multivalent, multispecific and modified nanobodies for disease treatment. Front Immunol. 2021;12:838082.
18. Lecocq Q, De Vlaeminck Y, Hanssens H, D'Huyvetter M, Raes G, Goyvaerts C, et al. Theranostics in immuno-oncology using nanobody derivatives. Theranostics. 2019;9(25):7772-91.
19. Yang XM, Lin XD, Shi W, Xie SX, Huang XN, Yin SH, et al. Nanobody-based bispecific T-cell engager (Nb-BiTE): a new platform for enhanced T-cell immunotherapy. Signal Transduct Target Ther. 2023;8(1):328.
20. Zhou S, Liu M, Ren F, Meng X, Yu J. The landscape of bispecific T cell engager in cancer treatment. Biomarker Res. 2021;9(1):38.
21. Belmontes B, Sawant DV, Zhong W, Tan H, Kaul A, Aeffner F, et al. Immunotherapy combinations overcome resistance to bispecific T cell engager treatment in T cell-cold solid tumors. Sci Transl Med. 2021;13(608):eabd1524.
22. Guo S, Deng CX. Effect of stromal cells in tumor microenvironment on metastasis initiation. Int J Biol Sci. 2018;14(14):2083-93.
23. Saleh R, Elkord E. Acquired resistance to cancer immunotherapy: role of tumor-mediated immunosuppression. Semin Cancer Biol. 2020;65:13-27.
24. Anderson NM, Simon MC. The tumor microenvironment. Curr Biol. 2020;30(16):R921-5.
25. Andrews LP, Yano H, Vignali DAA. Inhibitory receptors and ligands beyond PD-1, PD-L1 and CTLA-4: breakthroughs or backups. Nat Immunol. 2019;20(11):1425-34.
26. Zarour HM. Reversing T-cell dysfunction and exhaustion in cancer. Clin Cancer Res. 2016;22(8):1856-64.
27. Kurtulus S, Madi A, Escobar G, Klapholz M, Nyman J, Christian E, et al. Checkpoint blockade immunotherapy induces dynamic changes in PD-1(-)CD8(+) tumor-infiltrating T cells. Immunity. 2019;50(1):181-94.e6.
28. Huang Q, Wu X, Wang Z, Chen X, Wang L, Lu Y, et al. The primordial differentiation of tumor-specific memory CD8(+) T cells as bona fide responders to PD-1/PD-L1 blockade in draining lymph nodes. Cell. 2022;185(22):4049-66.e25.
29. Waite JC, Wang B, Haber L, Hermann A, Ullman E, Ye X, et al. Tumor-targeted CD28 bispecific antibodies enhance the antitumor efficacy of PD-1 immunotherapy. Sci Transl Med. 2020;12(549):eaba2325.
30. Yi M, Zheng X, Niu M, Zhu S, Ge H, Wu K. Combination strategies with PD-1/PD-L1 blockade: current advances and future directions. Mol Cancer. 2022;21(1):28.
31. Philip M, Schietinger A. CD8(+) T cell differentiation and dysfunction in cancer. Nat Rev Immunol. 2022;22(4):209-23.
32. Krupka C, Kufer P, Kischel R, Zugmaier G, Lichtenegger FS, Kohnke T, et al. Blockade of the PD-1/PD-L1 axis augments lysis of AML cells by the CD33/CD3 BiTE antibody construct AMG 330: reversing a T-cell-induced immune escape mechanism. Leukemia. 2016;30(2):484-91.
33. Herrmann M, Krupka C, Deiser K, Brauchle B, Marcinek A, Wagner AO, et al. Bifunctional PD-1 x alpha CD3 x alpha CD33 fusion protein reverses adaptive immune escape in acute myeloid leukemia. Blood. 2018;132(23):2484-94.
34. Rigamonti N, Veitonmaki N, Domke C, Barsin S, Jetzer S, Abdelmotaleb O, et al. A multispecific anti-CD40 DARPin construct induces tumor-selective CD40 activation and tumor regression. Cancer Immunol Res. 2022;10(5):626-40.
35. Saw PE, Chen JN, Song EW. Targeting CAFs to overcome anticancer therapeutic resistance. Trends Cancer. 2022;8(7):527-55.
36. Chen XM, Song EW. Turning foes to friends: targeting cancer-associated fibroblasts. Nat Rev Drug Discov. 2019;18(2):99-115.
37. Mao X, Xu J, Wang W, Liang C, Hua J, Liu J, et al. Crosstalk between cancer-associated fibroblasts and immune cells in the tumor microenvironment: new findings and future perspectives. Mol Cancer. 2021;20(1):131.
38. Kraman M, Bambrough PJ, Arnold JN, Roberts EW, Magiera L, Jones JO, et al. Suppression of antitumor immunity by stromal cells expressing fibroblast activation protein-alpha. Science. 2010;330(6005):827-30.
39. Brocks B, Garin-Chesa P, Behrle E, Park JE, Rettig WJ, Pfizenmaier K, et al. Species-crossreactive scFv against the tumor stroma marker "fibroblast

activation protein" selected by phage display from an immunized FAP-/- knock-out mouse. Mol Med. 2001;7(7):461-9.
40. Feig C, Jones JO, Kraman M, Wells RJ, Deonarine A, Chan DS, et al. Targeting CXCL12 from FAP-expressing carcinoma-associated fibroblasts synergizes with anti-PD-L1 immunotherapy in pancreatic cancer. Proc Natl Acad Sci U S A. 2013;110(50):20212-7.
41. Shi W, Yang X, Xie S, Zhong D, Lin X, Ding Z, et al. A new PD-1-specific nanobody enhances the antitumor activity of T-cells in synergy with dendritic cell vaccine. Cancer Lett. 2021;522:184-97.
42. Mo F, Duan S, Jiang X, Yang X, Hou X, Shi W, et al. Nanobody-based chimeric antigen receptor T cells designed by CRISPR/Cas9 technology for solid tumor immunotherapy. Signal Transduct Target Ther. 2021;6(1):80.
43. Sun S, Ding Z, Gao L, Hammock BD, Huang X, Xu ZP, et al. A dendritic/tumor fusion cell vaccine enhances efficacy of nanobody-based CAR-T cells against solid tumor. Theranostics. 2023;13(14):5099-113.
44. Zheng S, Wang J, Ding N, Chen W, Chen H, Xue M, et al. Prodrug polymeric micelles integrating cancer-associated fibroblasts deactivation and synergistic chemotherapy for gastric cancer. J Nanobiotechnol. 2021;19(1):381.
45. Xu M, Zhang P, Ding J, Chen J, Huo L, Liu Z. Albumin binder-conjugated fibroblast activation protein inhibitor radiopharmaceuticals for cancer therapy. J Nucl Med. 2022;63(6):952-8.
46. Tapia-Galisteo A, Compte M, Alvarez-Vallina L, Sanz L. When three is not a crowd: trispecific antibodies for enhanced cancer immunotherapy. Theranostics. 2023;13(3):1028-41.
47. Tapia-Galisteo A, Sanchez Rodriguez I, Aguilar-Sopena O, Harwood SL, Narbona J, Ferreras Gutierrez M, et al. Trispecific T-cell engagers for dual tumor-targeting of colorectal cancer. Oncoimmunology. 2022;11(1):2034355.
48. Austin RJ, Lemon BD, Aaron WH, Barath M, Culp PA, DuBridge RB, et al. TriTACs, a novel class of T-cell-engaging protein constructs designed for the treatment of solid tumors. Mol Cancer Ther. 2021;20(1):109-20.
49. Molloy ME, Austin RJ, Lemon BD, Aaron WH, Ganti V, Jones A, et al. Preclinical characterization of HPN536, a trispecific, T-cell-activating protein construct for the treatment of mesothelin-expressing solid tumors. Clin Cancer Res. 2021;27(5):1452-62.
50. Liu Y, Cao X. Immunosuppressive cells in tumor immune escape and metastasis. J Mol Med (Berl). 2016;94(5):509-22.
51. Marin-Acevedo JA, Kimbrough EO, Lou Y. Next generation of immune checkpoint inhibitors and beyond. J Hematol Oncol. 2021;14(1):45.
52. Yeku OO, Rao TD, Laster I, Kononenko A, Purdon TJ, Wang P, et al. Bispecific T-cell engaging antibodies against MUC16 demonstrate efficacy against ovarian cancer in monotherapy and in combination with PD-1 and VEGF inhibition. Front Immunol. 2021;12:663379.
53. Sam J, Colombetti S, Fauti T, Roller A, Biehl M, Fahrni L, et al. Combination of T-cell bispecific antibodies with PD-L1 checkpoint inhibition elicits superior anti-tumor activity. Front Oncol. 2020;10:575737.
54. Osada T, Patel SP, Hammond SA, Osada K, Morse MA, Lyerly HK. CEA/CD3-bispecific T cell-engaging (BiTE) antibody-mediated T lymphocyte cytotoxicity maximized by inhibition of both PD1 and PD-L1. Cancer Immunol Immunother. 2015;64(6):677-88.
55. Pei L, Liu Y, Liu L, Gao S, Gao X, Feng Y, et al. Roles of cancer-associated fibroblasts (CAFs) in anti- PD-1/PD-L1 immunotherapy for solid cancers. Mol Cancer. 2023;22(1):29.
56. Freedman JD, Duffy MR, Lei-Rossmann J, Muntzer A, Scott EM, Hagel J, et al. An oncolytic virus expressing a T-cell engager simultaneously targets cancer and immunosuppressive stromal cells. Cancer Res. 2018;78(24):6852-65.
57. Liu L, Chen J, Bae J, Li H, Sun Z, Moore C, et al. Rejuvenation of tumour-specific T cells through bispecific antibodies targeting PD-L1 on dendritic cells. Nat Biomed Eng. 2021;5(11):1261-73.